Available online at www.sciencedirect.com
ScienceDirect
Journal of Fluorine Chemistry 129 (2008) 204–209
JOURNAL OF FLUORINE CHEMISTRY
www.elsevier.com/locate/fluor

# Enhanced ultraviolet up-conversion emissions of $Tm^{3+}/Yb^{3+}$ codoped $YF_3$ nanocrystals

Chunyan Cao [b,c], Weiping Qin [a,b,*], Jisen Zhang [b], Yan Wang [b,c], Peifen Zhu [a], Guofeng Wang [a], Guodong Wei [a], Lili Wang [a], Longzhen Jin [a]

[a] State Key Laboratory on Integrated Optoelectronics, College of Electronic Science and Engineering, Jilin University, Changchun 130012, China
[b] Key Laboratory of Excited State Processes, Changchun Institute of Optics, Fine Mechanics and Physics, Chinese Academy of Sciences, Changchun 130033, China
[c] Graduate School of Chinese Academy of Sciences, Beijing 100049, China

Received 13 August 2007; received in revised form 25 October 2007; accepted 1 November 2007
Available online 21 December 2007

**Abstract**

$Tm^{3+}/Yb^{3+}$ codoped rod-like $YF_3$ nanocrystals were synthesized through a facile hydrothermal method. After annealing in an argon atmosphere, the nanocrystals emitted bright blue and intense ultraviolet (UV) light under a 980-nm continuous wave diode laser excitation. Up-conversion emissions centered at ~291 nm ($^1I_6 \rightarrow {}^3H_6$), ~347 nm ($^1I_6 \rightarrow {}^3F_4$), ~362 nm ($^1D_2 \rightarrow {}^3H_6$), ~452 nm ($^1D_2 \rightarrow {}^3F_4$), ~476 nm ($^1G_4 \rightarrow {}^3H_6$), ~642 nm ($^1G_4 \rightarrow {}^3F_4$), and ~805 nm ($^3H_4 \rightarrow {}^3H_6$) were recorded using a fluorescence spectrophotometer. Especially, enhanced UV emissions were studied by changing $Yb^{3+}/Tm^{3+}$ doping concentrations, the annealing temperatures, and the excitation power densities. A possible mechanism, energy transfer–cross relaxation–energy transfer (ET–CR–ET), was proposed based on a simple rate-equation model to elucidate the process of the enhanced UV emissions.


*Keywords:* Hydrothermal method; Ultraviolet up-conversion emissions; $Tm^{3+}/Yb^{3+}$ codoped $YF_3$; Rate-equation model; Energy transfer–cross relaxation–energy transfer

## 1. Introduction

In recent years, a subgroup of luminescent materials have been developed, which are capable of converting long wavelengths radiation into short wavelengths [1,2]. The emissions of most of these materials are based on up-conversion (UC) processes. The frequency UC in rare earth ions doped solids has been investigated extensively owing to its potential applications in a large range of areas including detection of infrared radiation [3], color display [4], UC lasers [5], medical applications, sensors, optical data storage, optoelectronics [2], and so on. Most of these applications are based on fluoride systems because they have appropriate energy phonons to produce strong UC fluorescence. The introduction of $Yb^{3+}$ as a sensitizer at around 1 μm pumping wavelength, where high-power sources are commercially available, allows a large enhancement of UC fluorescence of lanthanide ion activators, too. In $Yb^{3+}$ sensitized rare earth ions doped materials, efficient IR (NIR)-to-UV UC emissions have widely been investigated [6–9]. $Tm^{3+}$ is a promising optical activator that provides the possibility for simultaneous blue and UV emissions of laser action and various applications [10–15]. Especially, the phenomenon of UV UC luminescence has become an appealing research topic recently. Studies of new approaches to obtain efficient UV luminescence are very necessary and valuable due to the need for developing short-wavelength solid-state lasers.

In this article, $Tm^{3+}/Yb^{3+}$ codoped $YF_3$ nanoparticles were synthesized using a facile hydrothermal method. The annealed samples emitted bright UC light under 980-nm excitation. Particularly, the enhanced UV emissions were observed. The factors ($Yb^{3+}$ and $Tm^{3+}$ doping concentrations, annealing temperatures, and excitation power densities) resulting in enhanced UV UC emissions were studied and analyzed. A simple rate-equation model was established to explain the phenomena. A possible UV UC process based on frequency UC

* Corresponding author. Tel.: +86 431 85168240x8325; fax: +86 431 851682401/1x8325.
*E-mail address:* wpqin@jlu.edu.cn (W. Qin).

0022-1139/$ – see front matter © 2007 Elsevier B.V. All rights reserved.
doi:10.1016/j.jfluchem.2007.11.002

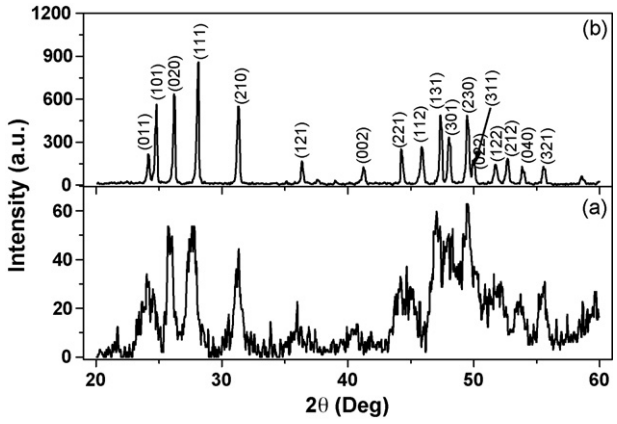


Fig. 1. XRD patterns of $Y_{0.797}Yb_{0.2}Tm_{0.003}F_3$: (a) before annealing, and (b) after annealing at 500 °C for 1 h.

mechanisms [2,16], energy transfer–cross relaxation–energy transfer (ET-CR-ET), was proposed and elucidated.

## 2. Results and discussion

The XRD patterns of the $Y_{0.797}Yb_{0.2}Tm_{0.003}F_3$ are shown in Fig. 1 for before (Fig. 1(a)) and after annealing at 500 °C for 1 h (Fig. 1(b)). All diffraction peaks can be easily indexed to those of the orthorhombic phase of $YF_3$ with space group Pnma (62) (JCPDS 74-0911). The intensification of peaks from the unannealed sample to the annealed sample indicated increased crystallinity, which could result in improved luminescence properties due to the reduction of defects and the efficient doping. From the patterns, we inferred that the sample was nanometer-sized before annealing, and became well-crystallized and larger in size after annealing, as shown in the FE-SEM images described below.

The FE-SEM images of $Y_{0.797}Yb_{0.2}Tm_{0.003}F_3$ are shown in Fig. 2. Fig. 2(a) and (b) are images of unannealed sample, and (c) and (d) are images of annealed sample, which correspond with Fig. 1(a) and (b), respectively. As shown in Fig. 2(a), the unannealed samples were rod-like morphologies, which were about 1 μm in length and 300 nm in diameter. Fig. 2(b) is an image of single unit of the unannealed sample, indicating that the rod-like structures were assemblies of numerous smaller rods. Most of the small rods were about 10 nm in diameter and 40 nm in length and lined up lengthways. The FE-SEM images of the sample annealed at 500 °C (Fig. 2(c)) showed that the annealing process did not make significant changes to the morphology of the nanoparticles, except that small rods changed to elongated particles and interlinked each other, and the higher magnification image in Fig. 2(d) proves that further.

Fig. 3 is an UC emission spectrum of the sample $Y_{0.797}Yb_{0.2}Tm_{0.003}F_3$ in the 270–870 nm wavelength range, recorded under 980-nm excitation with power density ≈ 100 W/cm$^2$. UC emissions centered at ~291 nm originating from $^1I_6 \rightarrow {}^3H_6$ transition, ~347 nm from $^1I_6 \rightarrow {}^3F_4$ transition, ~362 nm from $^1D_2 \rightarrow {}^3H_6$ transition, ~452 nm from $^1D_2 \rightarrow {}^3F_4$ transition, ~476 nm from $^1G_4 \rightarrow {}^3H_6$ transition, ~642 nm from $^1G_4 \rightarrow {}^3F_4$ transition, including ~805 nm from $^3H_4 \rightarrow {}^3H_6$ transition, were recorded.

To understand the *n*-photon UC processes well, we investigated the dependence of pumping power on the fluorescent emission. For an unsaturated UC process, the number of photons that is necessary to populating the upper

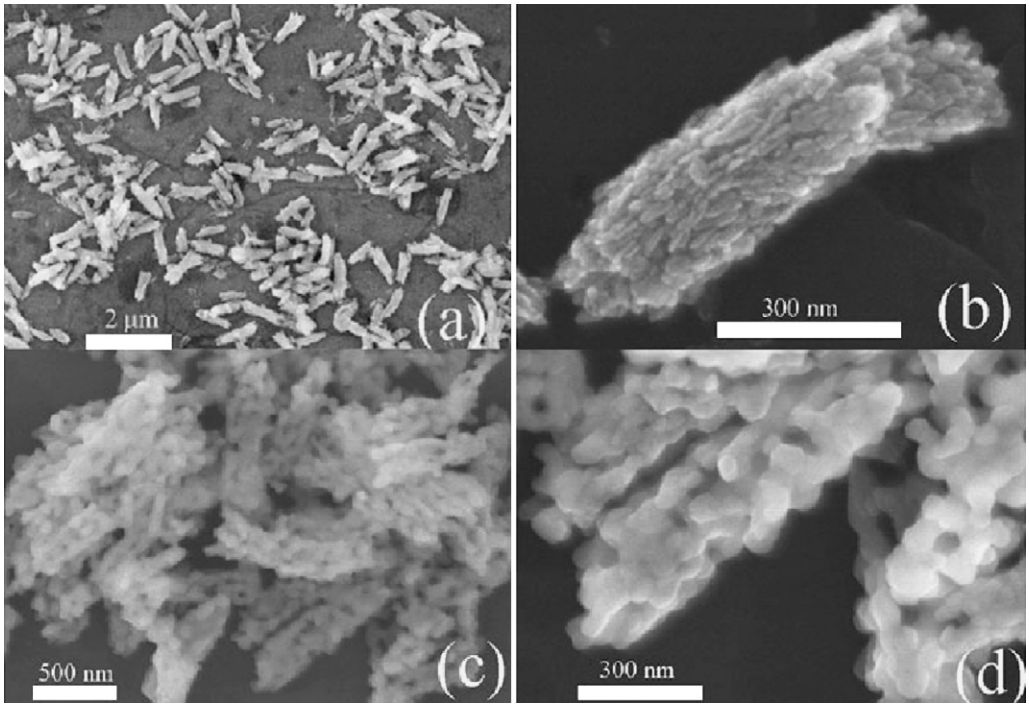


Fig. 2. FE-SEM images of $Y_{0.797}Yb_{0.2}Tm_{0.003}F_3$. Low magnification: (a) before annealing, and (c) after annealing at 500 °C for 1 h. High magnification: (b) single unit before annealing, and (d) after annealing.

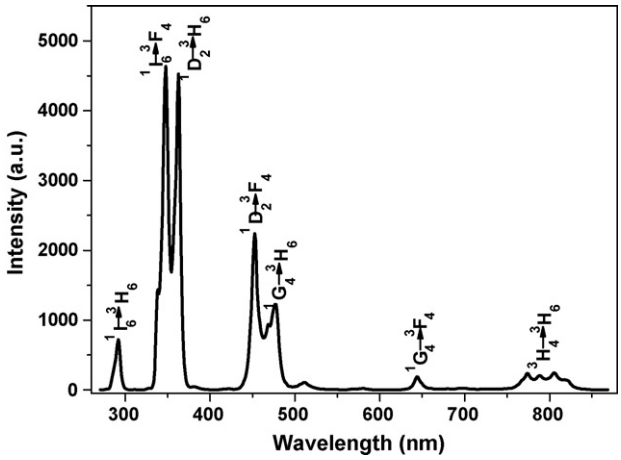


Fig. 3. Up-conversion emission spectrum of $Y_{0.797}Yb_{0.2}Tm_{0.003}F_3$ recorded under 980-nm excitation (power density ≈ 100 W/cm$^2$).

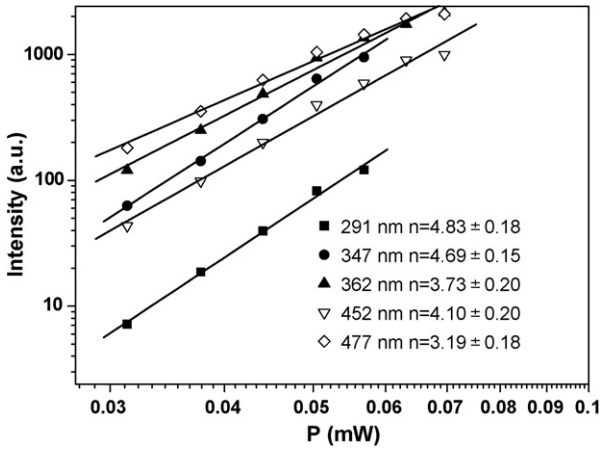


Fig. 4. Excitation power dependence of the fluorescence for $Y_{0.797}Yb_{0.2}Tm_{0.003}F_3$.

emitting state can be obtained by the following relation: $I_f \propto P^n$, where $I_f$ is the fluorescent intensity, $P$ the pumping laser power, and $n$ is the number of laser photons required [17]. The typical double-logarithmic plots of $\log I - \log P$ are shown in Fig. 4. The signal intensity of fluorescence is represented by the integrated area between the spectrum peak of profile and the baseline. The $n$ value is easily obtained from the slope of the linear fit. As illustrated in Fig. 4, $n$ value obtained for 477 nm was $3.19 \pm 0.18$, indicating a three-photon process. The $n$ values for 362 nm and 452 nm were $3.73 \pm 0.20$ and $4.10 \pm 0.20$, respectively, which meant that populating the $^1D_2$ level needs four photons. While for 347 nm and 291 nm emission, $n$ values were $4.69 \pm 0.15$ and $4.83 \pm 0.18$, respectively, meaning five-photon processes. The corresponding $n$ values of samples $Y_{0.8-y}Yb_{0.2}Tm_yF_3$ of the $\log I - \log P$ plots are listed in Table 1, which further prove that populating the $^1I_6$ level needs five photons, populating the $^1D_2$ level needs four photons, and populating the $^1G_4$ level needs three photons. The experimental results are slightly different from those in Refs. [8,9]. In the Refs., the authors believed that populating the $^1D_2$ level through cross relaxations (CR): $^3H_4 \rightarrow {}^3F_4$, $^1G_4 \rightarrow {}^1D_2$, and $^1G_4 \rightarrow {}^3F_4$, $^3H_4 \rightarrow {}^1D_2$, which needs five photons. We believed that the $^1D_2$ level was populated through the CR: $^3F_3 \rightarrow {}^3H_6$: $^3F_3 \rightarrow {}^1D_2$ ($Tm^{3+}$), bases on the Refs. [6,19], needing four photons.

As shown in Fig. 3, the emissions mainly concentrated on the blue, especially the UV bands, which meant that the five-, four-photon emissions were much stronger than those three-, or two-photon. What factors can result in the intense UV emissions? The enhanced UV UC emissions will be discussed in the following text. For comparison, the spectra were all recorded under the same conditions (excitation power density ~100 W/cm$^2$, high voltage of PMT = 400 V, Ex/Em slit = 1.0 nm), and normalized to the $^1G_4 \rightarrow {}^3H_6$ transition.

Table 1
Relevant $n$ values of the slopes for $\log I - \log P$ (nanocrystals $Y_{1-0.2-y}Yb_{0.2}Tm_yF_3$) plots

| $y$ | 291 nm | 347 nm | 362 nm | 452 nm | 477 nm |
|---|---|---|---|---|---|
| 0.1 | $4.82 \pm 0.28$ | $4.87 \pm 0.27$ | $4.24 \pm 0.21$ | $4.34 \pm 0.13$ | $3.24 \pm 0.19$ |
| 0.2 | $5.00 \pm 0.21$ | $4.76 \pm 0.24$ | $4.16 \pm 0.22$ | $4.27 \pm 0.19$ | $3.23 \pm 0.18$ |
| 0.3 | $4.83 \pm 0.18$ | $4.69 \pm 0.15$ | $3.73 \pm 0.20$ | $4.10 \pm 0.20$ | $3.19 \pm 0.18$ |
| 0.5 | $4.80 \pm 0.18$ | $4.91 \pm 0.19$ | $4.21 \pm 0.19$ | $4.18 \pm 0.11$ | $3.39 \pm 0.10$ |

$Yb^{3+}$ ions served as sensitizers in our studied system. The UC emission spectra dependence on sensitizers' concentration is shown in Fig. 5(a). With the increase of $Yb^{3+}$ concentration, $^1I_6 \rightarrow {}^3H_6$, $^1I_6 \rightarrow {}^3F_4$, $^1D_2 \rightarrow {}^3H_6$, and $^1D_2 \rightarrow {}^3F_4$ transitions relatively became stronger than the other UC processes and gradually became dominant. We concluded that high $Yb^{3+}$ concentration would result in the increase of the population of the $^1I_6$ and $^1D_2$ levels. And the enhanced UV UC emissions were observed. $Tm^{3+}$ ions act as activators. The spectra of the nanocrystals $Y_{0.8-y}Yb_{0.2}Tm_yF_3$ are shown in Fig. 5(b). We found that the spectra had the same changing trends with those of $Yb^{3+}$ ions. With the increase of $Tm^{3+}$ concentration, $^1I_6 \rightarrow {}^3H_6$, $^1I_6 \rightarrow {}^3F_4$, $^1D_2 \rightarrow {}^3H_6$, and $^1D_2 \rightarrow {}^3F_4$ transitions gradually became stronger and predominate over the $^1G_4 \rightarrow {}^3H_6$ transition. The annealing temperatures have great effect on the luminescence of the materials. The spectra of the sample $Y_{0.797}Yb_{0.2}Tm_{0.003}F_3$ annealed at 400 °C, 500 °C and 700 °C for 1 h are shown in Fig. 5(c). Clearly, with the increase of the annealing temperatures, the UV UC emissions had the enhancement phenomena, too. However, the annealing temperatures had much less effect on the UV UC emissions than $Yb^{3+}$ or $Tm^{3+}$ doping concentrations. Increasing the excitation power density has the same effect with that of increasing $Yb^{3+}$ concentration. The UC spectra of $Y_{0.797}Yb_{0.2}Tm_{0.003}F_3$ dependence on excitation power densities were investigated, too. The relative spectra are shown in Fig. 5(d). With the increase of excitation power densities, UV emissions became much stronger than the other UC ones, which meant that relatively high excitation power density led to the enhanced UV emissions, too.

To understand the enhanced UV UC emissions clearly, we plotted the emission intensity versus the variables in Fig. 6, where the intensity (summations of integrated areas of the transition bands $^1I_6 \rightarrow {}^3H_6$, $^1I_6 \rightarrow {}^3F_4$, $^1D_2 \rightarrow {}^3H_6$, and $^1D_2 \rightarrow {}^3F_4$) was normalized to the integrated intensity of

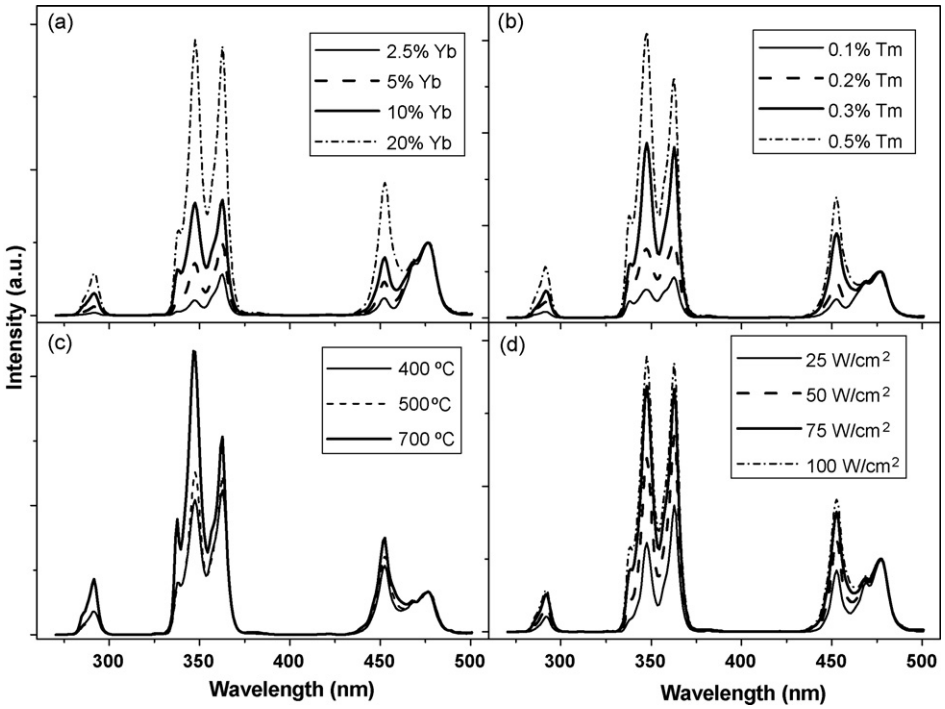


Fig. 5. Dependence of up-conversion emission spectra (normalized to $^1G_4 \rightarrow {}^3H_6$ transition) on (a) $Yb^{3+}$ concentration (nanocrystals $Y_{1-0.003-x}Yb_xTm_{0.003}F_3$), (b) $Tm^{3+}$ concentration (nanocrystals $Y_{1-0.2-y}Yb_{0.2}Tm_yF_3$), (c) annealing temperatures of nanocrystals $Y_{0.797}Yb_{0.2}Tm_{0.003}F_3$, and (d) excitation power densities of nanocrystals $Y_{0.797}Yb_{0.2}Tm_{0.003}F_3$.

$^1G_4 \rightarrow {}^3H_6$ transition. Obviously, all the variables had great effect on the UV UC emissions.

What is the possible UC mechanism resulting in enhanced UV UC emissions in $Tm^{3+}/Yb^{3+}$ codoped $YF_3$ system? Fig. 7 are schematic energy-level diagrams of $Yb^{3+}$ and $Tm^{3+}$. The UC mechanisms of the $Yb^{3+}$–$Tm^{3+}$ system are outlined in the figure, too. In $Tm^{3+}/Yb^{3+}$ codoped system, $Yb^{3+}$ ions successively transfer energy to $Tm^{3+}$ ions to populate the $^3H_5$, $^3F_3$ ($^3F_2$), and $^1G_4$ levels [18]. Due to the large energy mismatch ($\sim$3516 $cm^{-1}$) in the energy transfer (ET) $^2F_{5/2} \rightarrow {}^2F_{7/2}$ ($Yb^{3+}$): $^1G_4 \rightarrow {}^1D_2$ ($Tm^{3+}$), the CR $^3F_3 \rightarrow {}^3H_6$: $^3F_3 \rightarrow {}^1D_2$ ($Tm^{3+}$) may alternatively play an most important role in populating the $^1D_2$ level [6,19]. Then, the level $^1I_6$ is populated by the ET $^2F_{5/2} \rightarrow {}^2F_{7/2}$ ($Yb^{3+}$): $^1D_2 \rightarrow {}^1I_6$ ($Tm^{3+}$). The CR process depletes the population of the $^3F_3$ level; while the $Yb^{3+}$ ions successively transfer energy to $Tm^{3+}$ ions to populate the $^3F_3$ level, and CR process occur easily depleting the population of the $^3F_3$ level, which forms a loop (feedback). As a result, through ET–CR–ET process, the $^1D_2$ and $^1I_6$ levels can be efficiently populated, and the corresponding emissions become stronger. In order to understand the experimental results well, we used a rate-equation model, proposed by Auzel [20], and deduced by Ostermayer [21], to explain the experimental results. In the rate-equation model, the process of stepwise excitation by nonresonant ET from $Yb^{3+}$ to $Tm^{3+}$ and multiphonon relaxations of $Tm^{3+}$ were considered. As shown in Fig. 7, the labels listing left-hand are more

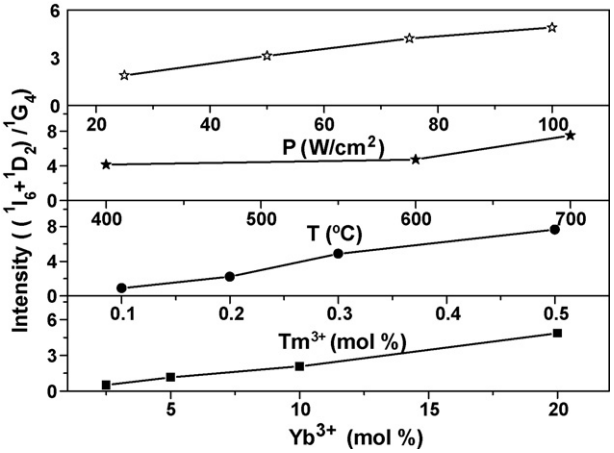


Fig. 6. Dependence of fluorescence (($^1I_6 + {}^1D_2$)/$^1G_4$) on $Yb^{3+}$ and $Tm^{3+}$ concentrations, annealing temperatures, and excitation power densities.

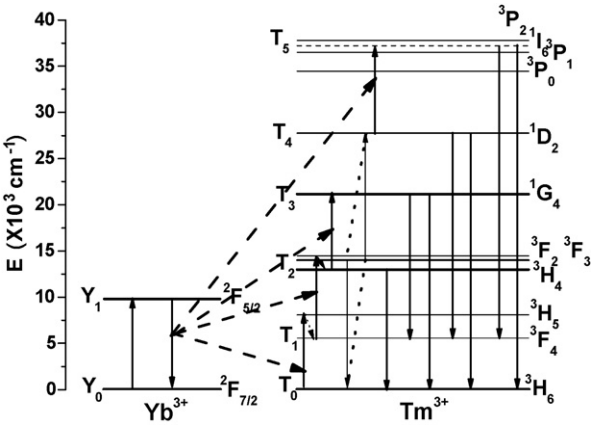


Fig. 7. Schematic energy-level diagram of $Yb^{3+}$ and $Tm^{3+}$, and mechanism of up-converted emissions.

conveniently used in the rate equations below:

$$\frac{dn_{Y1}}{dt} = \frac{\sigma_Y I}{\varepsilon_Y} n_{Y0} - \frac{n_{Y1}}{\tau_Y} - \chi_1 n_{Y1} n_{T0} - \chi_2 n_{Y1} n_{T1} - \chi_3 n_{Y1} n_{T2} - \chi_4 n_{Y1} n_{T4} \quad (1)$$

$$\frac{dn_{T1}}{dt} = \chi_1 n_{Y1} n_{T0} - \frac{n_{T1}}{\tau_{T1}} - \chi_2 n_{Y1} n_{T1} \quad (2)$$

$$\frac{dn_{T2}}{dt} = b\chi_2 n_{Y1} n_{T1} - \frac{n_{T2}}{\tau_{T2}} - \chi_3 n_{Y1} n_{T2} \quad (3)$$

$$\frac{dn_{T3}}{dt} = \chi_3 n_{Y1} n_{T3} - \frac{n_{T3}}{\tau_{T3}} \quad (4)$$

$$\frac{dn_{T4}}{dt} = c(1-b)\chi_2 n_{Y1} n_{T1} (1-b)\chi_2 n_{Y1} n_{T1} - \frac{n_{T4}}{\tau_4} \quad (5)$$

$$\frac{dn_{T5}}{dt} = \chi_4 n_{Y1} n_{T4} - \frac{n_{T5}}{\tau_5} \quad (6)$$

where $\sigma_Y$ is the $Yb^{3+}$ $^2F_{7/2} \rightarrow {}^2F_{5/2}$ absorption cross section averaged over the spectrum of the exciting radiation, $\varepsilon_Y$ the average energy of the $Yb^{3+}$ $^2F_{7/2} \rightarrow {}^2F_{5/2}$ transition, $I$ the total intensity of the exciting radiation, the *n's* are number density of ions in the levels, the $\tau$*'s* are total lifetime of the levels, the $\chi$*'s* are the $Yb^{3+}$-to-$Tm^{3+}$ transfer probability coefficient, $b$ the branch ratio of the $^3F_3$ level relaxing to the $^3H_4$ level, and $c$ is CR coefficient. Herein, $\chi$*'s* increase monotonically with $Yb^{3+}$ concentration at low $Yb^{3+}$ concentration, while they take nearly constant value at high $Yb^{3+}$ concentration [22]. With the increase of $Tm^{3+}$ concentration, CR process becomes stronger for $Tm^{3+}$–$Tm^{3+}$ distance becomes smaller, $b$ becomes smaller, too, and there are some inevitable relations between $b$ and $c$. In the above rate equations, some approximations have been made. Firstly, low efficiency processes, such as back energy transfer from $Tm^{3+}$ to $Yb^{3+}$, were neglected in the rate-equation model. Secondly, in the ET and nonradiative processes, we assumed that the $^3H_5$ level completely depopulated to the $^3F_4$ (T1) level; $Tm^{3+}$ ions in the $^3F_3$ ($^3F_2$) level partially non-radiatively decayed to the level $^3H_4$ (T2), and the others depopulated via the CR ($^3F_3 \rightarrow {}^3H_6$: $^3F_3 \rightarrow {}^1D_2$) process; the $^1G_4$ (T3) level was populated via ET ($^2F_{5/2} \rightarrow {}^2F_{7/2}$ ($Yb^{3+}$): $^3H_4 \rightarrow {}^1G_4$ ($Tm^{3+}$)); the population of the $^1D_2$ (T4) level came only from the CR process; and the population of the $^1I_6$ (T5) level came from ET $^2F_{5/2} \rightarrow {}^2F_{7/2}$ ($Yb^{3+}$): $^1D_2 \rightarrow {}^1I_6$ ($Tm^{3+}$). Thirdly, other emission and ET processes were neglected except those mentioned above.

Now, we use the rate equation model to explain the enhanced UV UC emissions. First, for the dependence of the UC emission spectra on $Yb^{3+}$ concentration, $\chi$*'s* increased with $Yb^{3+}$ concentration increasing, ET became efficient and more $Yb^{3+}$ participated in the ET inducing more $Tm^{3+}$ to populate the $^3F_3$ ($^3F_2$) levels, the CR process easily happened, and then the populations of the levels $^1D_2$ and $^1I_6$ increased. So the enhanced UV emissions from $^1D_2$ and $^1I_6$ were observed. Second, $Tm^{3+}$ concentration had great effect on the $Tm^{3+}$ emissions as shown in Fig. 5(b). With the increase of $Tm^{3+}$ concentration, indicating the shorter distance between $Tm^{3+}$–$Tm^{3+}$, $Tm^{3+}$–$Tm^{3+}$ interaction became stronger, CR process happened easily. $Tm^{3+}$–$Yb^{3+}$ distance became shorter and ET happened easily, too, and the ET–CR–ET would be more effective, which resulted in UV emission enhancement. Third, increasing the annealing temperatures while keeping the doping concentration invariable, more $Yb^{3+}$ and $Tm^{3+}$ would be incorporated in the host lattices and the practical distance of $Yb^{3+}$ and $Tm^{3+}$ became shorter, resulting in the relatively effective ET and CR processes, which at last resulted in the UV emission enhancement phenomena. Last, for the UC emission spectra dependence on excitation power density, a likely explanation was given. When the excitation power density increased, the $Yb^{3+}$ would be more effectively excited to the $^2F_{5/2}$ level, and the ET processes became effective too. In a word, the ET–CR–ET eventually resulted in the enhanced emissions of the $^1D_2$ and $^1I_6$ levels.

## 3. Conclusions

In conclusion, $Tm^{3+}$/$Yb^{3+}$ codoped rod-like $YF_3$ nanocrystals were synthesized through a facile hydrothermal method. After annealing in an argon atmosphere, the nanocrystals had IR to UV UC emissions under 980-nm excitation. Particularly, bright blue and intense UV UC emissions were observed and studied. Increasing $Yb^{3+}$ and $Tm^{3+}$ doping concentration, annealing temperatures, including the excitation power densities, resulted in enhanced UV UC emissions of the nanocrystals. A simple rate-equation model was used under some approximations. The possible UV UC process, ET–CR–ET, was proposed and elucidated resorting to the simple rate-equation model. The elucidation was just qualitative. The quantitative explanation is under extensively study.

## 4. Experimental

The starting materials were all analytical reagents. In a typical procedure for the preparation of $Y_{0.797}Yb_{0.2}Tm_{0.003}F_3$, 7.97 mmol $Y_2O_3$, 2 mmol $Yb_2O_3$, and 0.03 mmol $Tm_2O_3$ were dissolved in the hydrochloric acid (37%) at elevated temperature to form clear solution. Then hydrofluoric acid (40%) was added dropwise into the clear solution to form colloidal solution while stirring with a magnetic force stirrer. After vigorously stirred for more than 0.5 h, the colloidal solution was transferred to four 50 mL Teflon-lined stainless steel autoclaves and treated at 130 °C for 12 h. After cooling to room temperature naturally, the upper clear solution was discarded and the remainder was isolated via centrifugation. The resultant material was dried in vacuum at 55 °C for 6 h. However, it had hardly UC luminescence under 980-nm excitation. After annealing at 500 °C for 1 h in an argon atmosphere, the sample emitted bright blue and intense UV light. Samples $Y_{0.997-x}Yb_xTm_{0.003}F_3$ ($x = 0.025$, 0.05, 0.10) and $Y_{0.8-y}Yb_{0.2}Tm_yF_3$ ($y = 0.001$, 0.002, 0.003, 0.005) were prepared in a similar manner to that for nanocrystals $Y_{0.797}Yb_{0.2}Tm_{0.003}F_3$. Furthermore, the $Y_{0.797}Yb_{0.2}Tm_{0.003}F_3$ nanoparticles were annealed at 400 °C, and 700 °C for 1 h for

the study of UC emission dependence on annealing temperatures.

The phase purity and composition identification were performed by powder X-ray diffraction (XRD) (Model Rigaku RU-200b), using nickel-filtered Cu Kα radiation (λ = 1.5406 Å). The size and morphology were characterized by field emission scanning electron microscopy (FE-SEM) (Hitachi S-4800). With a 980-nm continuous wave diode laser (CW LD 2W) as excitation source, UC emission spectra were recorded by a fluorescence spectrophotometer (Hitachi F-4500). All measurements were performed at room temperature.

## Acknowledgement

This work is supported by National Science Foundation of China under Grant Nos. 10474096 and 50672030.

## References

[1] F. Auzel, Proc. IEEE 61 (1973) 758–787.
[2] F. Auzel, Chem. Rev. 104 (2004) 139–173.
[3] R. Balda, A.J. Garcia-Adeva, M. Voda, J. Fernandez, Phys. Rev. B69 (2004) 205203–205210.
[4] E. Downing, L. Hesselink, J. Ralston, R. Macfarlane, Science 273 (1996) 1185–1187.
[5] S. Sanders, R.G. Waarts, D.G. Mehuys, D.F. Wetch, Appl. Phys. Lett. 67 (1995) 1815–1817.
[6] R.J. Thrash, L.F. Johnson, J. Opt. Soc. Am. B 11 (1994) 881–885.
[7] T. Riedener, H.U. Güdel, G.C. Valley, R.A. McFarlane, J. Lumin. 63 (1995) 327–337.
[8] X.B. Chen, Z.F. Song, J. Opt. Soc. Am. B 24 (2007) 965–971.
[9] G.Y. Chen, G. Somesfalean, Z.G. Zhang, Q. Sun, F.P. Wang, Opt. Lett. 32 (2007) 87–89.
[10] W.T. Carnall, R. Fields, K.T. Rajnank, J. Chem. Phys. 49 (1968) 4424–4442.
[11] J.J. Owen, A.K. Cheetham, R.A. Mcfarlane, J. Opt. Soc. Am. B 15 (1998) 684–693.
[12] M.P. Hehlen, A. Kuditcher, A.L. Lenef, H. Ni, Q. Shu, S.C. Rand, J. Rai, S. Rai, Phys. Rev. B 61 (2000) 1116–1128.
[13] J. Qiu, Y. Kawamoto, J. Fluorine Chem. 110 (2001) 175–180.
[14] I.R. Martin, J. Mendez-Ramos, V.D. Rodriguez, J.J. Romero, J. Garcia-Sole, Opt. Mater. 22 (2003) 327–333.
[15] G.S. Qin, W.P. Qin, C.F. Wu, S.H. Huang, D. Zhao, J.S. Zhang, S.Z. Lu, Opt. Commun. 242 (2004) 215–219.
[16] S. Sivakumar, F.C.J.M. van Veggel, P.S. May, J. Am. Chem. Soc. 129 (2007) 620–625.
[17] M. Pollnau, D.R. Gamelin, Phys. Rev. B 61 (2000) 3337–3346.
[18] F. Auzel, C. R. Acad. Sci. Paris 1016 (1966).
[19] M.A. Noginov, M. Curley, P. Venkateswarlu, A. Williams, H.P. Jenssen, J. Opt. Soc. Am. B 14 (1997) 2126–2136.
[20] F. Auzel, Compt. Rend. Acad. Sci. 263B (1966) 819–821.
[21] F.W. Ostermayer, J.J.P. Van der ziel, H.M. Marcos, L.C. Van Uilert, J.E. Geusic, Phys. Rev. B 3 (1970) 2698–2705.
[22] Y. Mita, T. Ide, M. Togashi, H. Yamamoto, J. Appl. Phys. 85 (1999) 4160–4164.